



## RESEARCH PAPER

## OPEN ACCESS

## Chemical route synthesis of MgO nanoparticles for the enhanced photocatalytic performance and antimicrobial studies

C. Karthika<sup>1</sup>, N. Subha<sup>1</sup>, SP. Manobala<sup>1</sup>, M. Sakthi Bagavathy<sup>1</sup>, S. Rajaduraipandian<sup>2</sup>, S. Gandhimathi<sup>2</sup>, J. Jenson Samraj<sup>1</sup>; Annadurai Gurusamy\*<sup>1</sup>

<sup>1</sup>*Division of Nanoscience, Sri Paramakalyani Centre of Excellence in Environmental Sciences, Manonmaniam Sundaranar University, Alwarkurichi, India*

<sup>2</sup>*Sri Paramakalyani College, Manonmaniam Sundaranar University, Alwarkurichi, India*

Article published on December 06, 2021

**Key words:** MgONPs, Co-precipitation method, TGA, Photocatalytic activity, Antibacterial activity

### Abstract

The present study was carried out to synthesize magnesium oxide nanoparticles (MgONPs) through the co-precipitation method using Magnesium chloride as a precursor for the photodegradation of Rhodamine B dye (RhB) and the antibacterial studies against *E. coli*. The as-synthesized nanoparticles are characterized by XRD, FT-IR, TGA, DLS, SEM, and PL. XRD displayed the crystallinity of MgONPs with an average crystalline size of 29nm. Morphology of MgONPs exhibited a rod-like shape. Photocatalytic activity of MgONPs was witnessed by the quick degradation of the organic dye RhB on exposure with both sunlight and UV irradiation and the antibacterial activity of MgONPs was found effect against *E. coli* at the concentrations ranging from 40 - 100µg/ml respectively. The maximum ZOI (2.6) was observed at the concentration of 100µl. Furthermore, the MgONPs could be used in the remediation of polluted water and for biomedical applications.

\*Corresponding Author: Annadurai Gurusamy ✉ [gannadurai@msuniv.ac.in](mailto:gannadurai@msuniv.ac.in)

## Introduction

At present, organic pollutants in aquatic ecosystems due to the rapid increase in population, industrialization, and ongoing development of technologies have been considered the most significant environmental crises in all developing countries (Elimelech and Phillip, 2011; Santhosh *et al.*, 2016; Tauseef Munawari *et al.*, 2021). Recently, nanosciences and nanotechnology have been leading to a technological revolution in the world, which is concerned with materials with significantly novel and improved physical, chemical, and biological properties. In this regard, nanoparticles are recognized as antibacterial agents due to their size, structure, and surface properties. Thus, nanotechnology offers a way to improve the activity of inorganic antibacterial agents. Nanosize materials have different properties compared with bulk materials. Nanoparticles are particles between 1 to 100 nanometers in size and it has attracted great attention in recent years because of their unique electronic, physical, magnetic, chemical, and optical properties compared with bulk materials. Nanoparticles are generally prepared by wet chemical, mechanical, form-in-place, and gas-phase synthesis methods. There are two broad areas for the synthesis of nanostructured materials including physical methods and chemical methods. Some of the commonly used physical and chemical methods are inert gas evaporation, ion sputtering, solvothermal synthesis, chemical vapor deposition, reduction, and sol-gel technique are not found toxic to the environment. Different physicochemical techniques have been adopted to synthesize MgONPs such as precipitation, chemical vapor deposition, solvothermal, microwave combustion, sonochemical methods, etc. (Veldurthi *et al.*, 2012; Zhao *et al.*, 2011; Li *et al.*, 2013; Alvai and Morsali, 2010; Al-Gaashani *et al.*, 2016; Selvam *et al.*, 2011; Sun *et al.*, 2008).

Currently, metal oxide nanoparticles have gained significant interest among scientists as potential adsorbents for the removal of dyes from wastewater (Mahato *et al.*, 2009) due to their high surface area, large number of active sites, high surface to volume

ratio, and unusual lattice planes. Among all known metal oxide nanoparticles, MgONPs has become a distinctive material because of their uniqueness in high ionic character, crystal structure, simple stoichiometry, and its novelty in different applications, such as electronics, adsorption, catalysis, and many other fields (Sathyamoorthy *et al.*, 2013; Yuan *et al.*, 2011). Some metal oxides can act as nano adsorbents like ZnO, SnO<sub>2</sub>, Fe<sub>2</sub>O<sub>3</sub>, etc. (Maiti *et al.*, 2017). In this work, the MgONPs were prepared as a photocatalyst using the co-precipitation method and utilized for degrading RhB from an aqueous solution. The antibacterial activity was observed as dose-dependent damaging of gram-negative bacteria with a suitable zone of inhibition.

## Material and methods

### Materials

Chemicals including magnesium nitrate hexahydrate (Mg(NO<sub>3</sub>)<sub>2</sub>·6H<sub>2</sub>O; 99.9%) and Rhodamine B C<sub>28</sub>H<sub>31</sub>ClN<sub>2</sub>O<sub>3</sub> were acquired from Sigma-Aldrich. For experimental work, double-distilled de-ionized water was utilized. All reagents used in the present work were purchased from Sigma-Aldrich (Poland). Milli-Q water was used throughout the experiment. All the reagents utilized during the experimental process were of analytical grade.

### Preparation of MgONPs

MgONPs were prepared through the co-precipitation route using Magnesium dichloride, Potassium hydroxide, and Sodium hydroxide used as a surfactant at room temperature. Then 50ml of 1M solution of Potassium hydroxide was slowly added to it using addition funnel drop by drop under constant stirring condition. Similarly, Magnesium dichloride solution was prepared by dissolving Magnesium dichloride in distilled water and kept above in the magnetic stirrer and allowed to stir for 10-20 minutes, at room temperature. Then 50ml of 1M NaOH solution was slowly added into the above resulting solution under stirring. This whole process was carried out under constant vigorous stirring conditions (140 rpm). After the addition precipitating agent the constituent mixture was allowed to stir for 5

hrs without altering any parameters. After completion of this whole reaction process, very finely powdered white precipitate MgO was prepared. The whole precipitation was washed thoroughly with the help of doubly distilled water to make the precipitate free from tracer of foreign elements. Then the MgONPs were obtained via a controlled calcination process using a muffle furnace for 4 hrs at 450 °C.

#### Antibacterial activity

The ZOI (the region where the bacterial growth was inhibited owing to the presence of the MgONPs) was recorded for numerous samples of MgONPs prepared under different conditions. The sample of MgO Nps produced at the optimized conditions exhibited good results against the strain of *E. coli*. An increment in the concentration of the MgONPs positively affected the antimicrobial potential and increased the value of ZOI (Ibrahim *et al.*, 2017).

### Result and discussion

#### X-ray Diffraction

Fig 1. shows the X-ray diffraction pattern of the samples annealed at 300-500°C for 4 hours in the furnace. The observed diffraction peaks are well-matched with the typical single-crystalline periclase phase of bulk MgO and are also in good agreement with the JCPDS file for MgO (JCPDS Card No. 01-076-1363) (Saket *et al.*, 2021). The MgONP displayed crystalline peaks at  $2\theta$  values of 37.74°, 40.73°, 58.83°, 66.52°, 73.81° are assigned to the MgO crystal planes of (200), (210), (221), (222), and (321) respectively. The intense sharp peaks in this pattern reveal the high crystalline nature of the MgONPs.

The crystalline size of the MgONPs was measured as 29nm through the well-known Debye Scherrer formula. Almost similar XRD results were reported for MgONPs prepared by other biogenic materials (Pugazhendhi *et al.*, 2019). Similarly, diffractions at 36.7, 42.71, and 62.0 were detected and attributed to the MgO structure (Tadjarodi *et al.*, 2012).

Furthermore, it has been reported that when two or more metals are combined, the optical properties of the MONPs may be affected by an excess of doping

material (Tadjarodi *et al.*, 2012; Lopez *et al.*, 2009; Perez-Larios *et al.*, 2012; Das *et al.*, 2013).

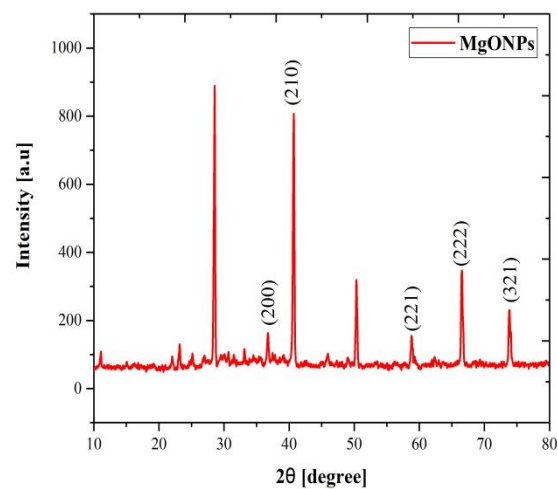


Fig. 1. XRD pattern of the synthesized MgONPs.

#### Fourier Transform Infrared Spectroscopy

Fourier transform infrared (FTIR) spectroscopy is based on the chemical bonds in a molecule that vibrates at characteristic frequencies depending on the elements and types of bonds. During FTIR measurements, a spot on the specimen is subjected to a modulated IR beam.

The transmittance and reflectance of the infrared radiation at different frequencies are measured and translated into an IR absorption plot. The resulting FTIR spectral pattern was analyzed and matched with known signatures peaks of identified materials in the FTIR library.

The composition of the sample was analyzed by the FTIR measurement as depicted in Fig 2. The synthesized powder was mixed with KBr and the pellet of the mixture was used for infrared (IR) spectroscopic measurement at room temperature while the wavelength was varied from 400 to 4000  $\text{cm}^{-1}$ . The absorption band at 3317  $\text{cm}^{-1}$  indicates the bending mode of vibration in water (NH).

The band at 1622  $\text{cm}^{-1}$  corresponds to C=O stretching. The peak at 1522  $\text{cm}^{-1}$ , 1429  $\text{cm}^{-1}$ , and 1150  $\text{cm}^{-1}$  are C=C,  $\text{CH}_2$ , and C-OH. The broad peak at 565  $\text{cm}^{-1}$  shows the formation of MgONPs.

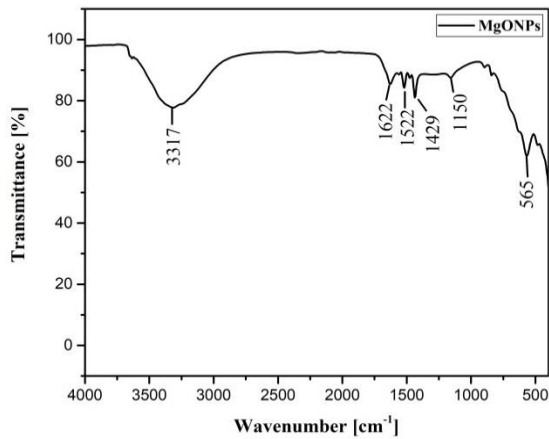


Fig. 2. FT-IR spectrum of the synthesized MgONPs.

*Thermal gravimetric analysis*

The decomposition temperature of the material was investigated using thermogravimetric analysis (TGA) as shown in Fig 3. The TGA curve of MgONPs was obtained in normal atmospheric conditions, with a heating rate of 10°C/min. The analysis indicated the loss of mass occurred in two steps, in which the first step is from 50°C to 320°C, which may be due to the liberation of the water molecules adsorbed on the surface. The second step comes in the range of 103°C-300°C, which may be attributed to the dehydroxylation of Mg (OH)<sub>2</sub>, signifying the decomposition of Mg (OH)<sub>2</sub> to MgONPs (Barsharani Priyadarshini *et al.*, 2021). Thermogravimetric analysis is a technique by which we can measure the mass loss concerning temperature. Fig 3 shows the weight loss of the MgONP powder sample. Primary weight loss of ~ 11.92% was observed at 103°C due to solvent evaporation. Phase transition is found to occur at about 300°C indicating the transition from magnesium hydroxide to magnesium oxide with weight loss of ~ 15-19%.

The major weight losses occur at about 400°C and two minor ones at lower and higher temperatures. The TGA curve of MgONPs shows two-step dehydration in the range of 103–300°C, corresponding to the desorption of the surface-bound water (11.92%) and the dihydroxylation process 15-19% Overall, TGA supports the expected degree of functionalization and also shows good stability of the material up to 463°C. (Muhammad Isa Khan *et al.*, 2020).

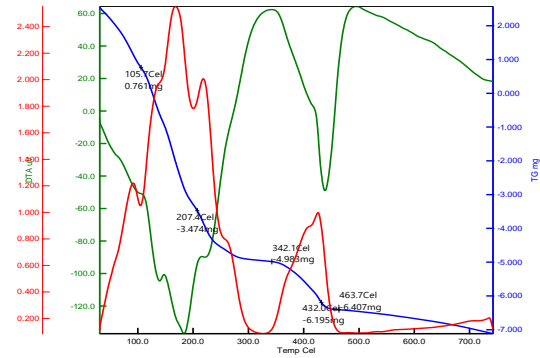


Fig. 3. TGA of the synthesized MgONPs.

*Dynamic Light Scattering*

The particle size of MgONPs was analyzed by DLS using a particle size analyzer as depicted in Fig 4 based on hydrodynamic diameter. Histogram of intensity distribution shows the average hydrodynamic diameter of 5.8nm. The Polydispersity index (PDI) was 0.4981 indicates monodispersed of the particles.

The size was further revealed by SEM analyses and the surface charge of the nanoparticles was responsible during interaction with molecules more particularly biological systems such as plants, which should normally be in the range of -30 to +30 mV. DLS was performed to determine the hydrodynamic size (diameter) of the synthesized MgONPs as depicted in Fig 4. However, MgONPs used in this study have an average diameter of 2.8nm corresponds to 0.4981 (PDI) which is monodispersed (Ramesh Raliya *et al.*, 2014).

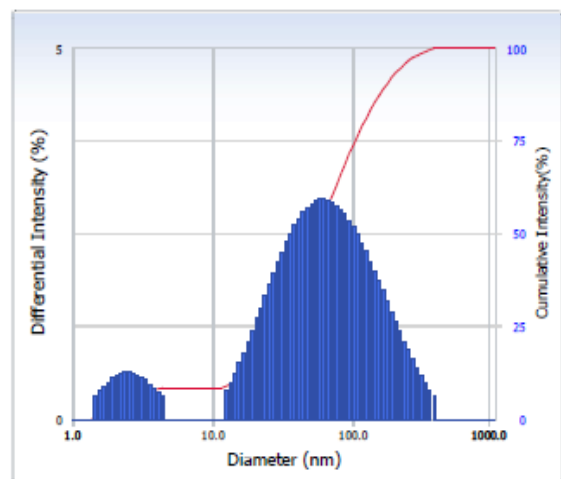
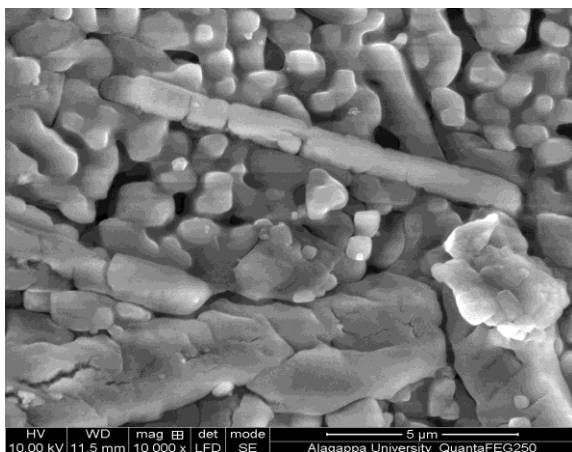


Fig. 4. DLS of the synthesized MgONPs.

### Scanning Electron Microscopy

SEM study was applied to study the morphological and structural data of the prepared nanomaterial. SEM images of MgONPs (Fig. 5) exhibited rod-like structures with agglomeration due to the aggregation of several nanoparticles. Sharma *et al.* (2017) found the morphology of MgONPs as spherical with minimal variations in size or shape, such as oval and elliptical particles. The particles appeared agglomerated and some of the spherical particles are observed integrated to form rod-like structures. Mageshwari *et al.*, 2013 and Karthika *et al.*, 2018 reported that the morphology of the rod shape would be controlled by hydrothermal conditions. The obtained rod-shaped morphology could be used in biomedical applications as it could reside for a longer duration in the blood circulation.



**Fig. 5.** SEM micrographs of the synthesized MgONPs.

### Photoluminescence spectrum

The photoluminescence (PL) emission excitation spectrum of MgONPs recorded at room temperature as shown in Fig 6. In semiconductors, the recombination of the photo-generated free charge carriers leads to photoluminescence emission. The spectrum mainly shows two emission bands: (i) the UV excitonic emission and (ii) the level of the visible defect emission. Several authors have reported such excitonic and visible emissions for nano ZnO material (Dijken *et al.*, 2000; Hvam, 1978; Li *et al.*, 2000; Vanheusden *et al.*, 1996). The Near-Band-Edge (NBE) excitation peak at 350nm was recorded at an emission wavelength of 525nm. The emission

spectrum monitored at 350nm wavelength for MgONPs showed a broad yellow emission at 525nm. The broad 525nm peak was due to the transition between single charged oxygen vacancy and the photoexcited holes in the valence band of the MgONPs (Danith *et al.*, 2015; Nicolas *et al.*, 2014; Devaraja *et al.*, 2014). The color clarity of any luminescent material was expressed in terms of chromaticity coordinates, called Commission International De l'Eclairage. The energy levels of these defect centers exist in the forbidden energy gap of MgONPs. The variation in emission intensity due to the presence of a higher density of defects, methods of preparation, particle size effect, etc. (Gu *et al.*, 2006). These values were compared with the literature using a time-resolved spectrum (Prashantha *et al.*, 2012).

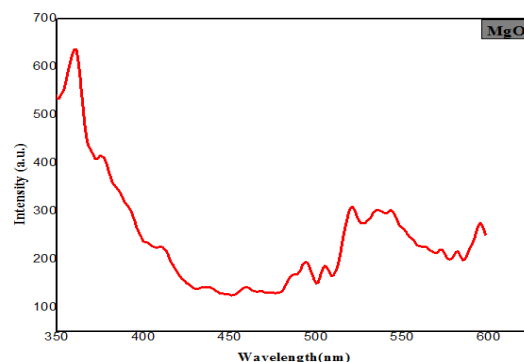


**Fig. 6.** PL spectrum of the synthesized MgONPs.

### Photocatalytic Studies

The photocatalytic activity of MgONP powder was measured by the photodegradation of RhB (model pollutant) under UV light and the results are presented in Fig 7. The intensity of the RhB peak at around 550nm decreased with increasing the UV exposure time indicated the degradation of dye under UV-irradiation. Approximately 90% of the RhB dye was degraded by the hybrid within 80min. The improved photocatalytic activity results from the good distribution of MgONPs allow for a semiconductor-semiconductor junction which resulted in a significantly enhanced photodegradation (Arivalagan Pugazhendhi, *et al.*, 2019). The photodegradation of a dye in an aqueous solution is due to the excitation of a semiconductor by UV light to produce free radicals

which aid in the degradation of the dye. The UV-irradiation excited the electrons from the valence band to its conduction band, generating high-energy electron-hole pairs to undergo continuous charge transfer to adsorbed species on the semiconductor surface resulting in a heterogeneous photocatalysis (Pugazhendhi *et al.*, 2019).

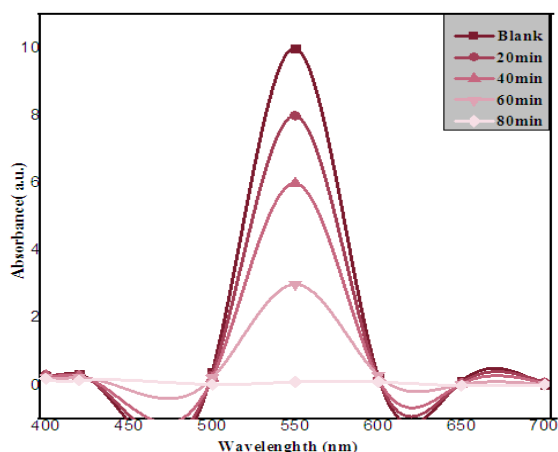


**Fig. 7.** Photocatalytic activity of the synthesized MgONPs.

#### Mechanism of Photodegradation

When MgO nanopowder is dispersed in the solution with selected dye, the surface electrons on MgONPs should eventually transfer to the dye, and when it is irradiated by UV light, electrons ( $e^-$ ) in the valence band (VB) can be excited to the conduction band (CB) with simultaneous generation of the same amount of holes in the VB. Similarly, the photo-induced holes can be easily trapped by  $\text{OH}^-$  to produce hydroxyl radical species ( $\text{OH}^\bullet$ ) further, which is an extremely strong oxidant for the partial or complete mineralization of organic pollutants (Meshko *et al.*, 2001; Min *et al.*, 2012). The following are the suggested reactions responsible for the degradation of the dye using MgONPs (Min *et al.*, 2012; Yan-Fen Lee *et al.*, 2011). It should be considered that the modification of the MgO surface would provide an effective environment for increasing the surface-active sites for the dye–semiconductor interaction, which in turn may increase the photodegradation processes. In addition, chitosan itself adsorbs dye molecules, which will be continuously supplied to

MgONPs for degradation, and thus contributes to increasing the efficiency of MgONPs significantly shown in Fig 8.

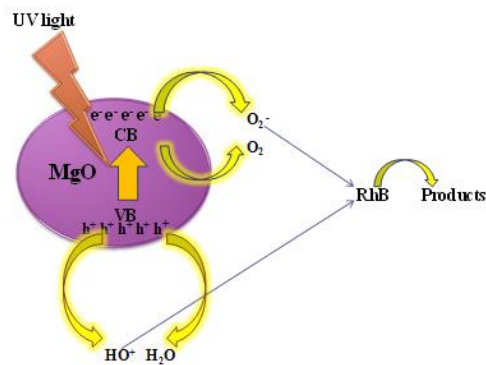


**Fig. 8.** Photodegradation mechanism of the synthesized MgONPs.

#### Antibacterial activity of MgONPs

The antibacterial property of the treated samples showed effective antibacterial properties against gram-negative bacteria, *E. coli* with the control. MgONPs have shown much better control over the growth of *E. coli*. The maximum zone of inhibition was found at 100 $\mu\text{l}$  (2.6mm). Fig 9 shows the difference in the zone of inhibition of *E. coli* with the increase in concentration. MgONPs inhibit the growth of *E. coli* by using an electrochemical mode of action. When MgONPs penetrate the cell wall, leakage of metabolites occurs and other cell functions are stopped, thereby preventing the organism from functioning or reproducing (Venkatasubramanian *et al.*, 2008; Shi *et al.*, 2014). The result indicated that the good reduction in the growth of *E. coli* confirmed the enhanced antibacterial activity of the MgONPs as shown in Table 1. The *E. coli* tended to be inactivated similarly regarding the time of treatment and the antimicrobial mechanism of MgONPs was attributed to the interaction with the strongly electronegative microbial surface. Moreover, MgONPs showed enhanced antibacterial activity which perhaps attributed to the synergistic effect. It was noteworthy, that the gram-negative bacteria have a thin layer of peptidoglycan and a more complex cell wall with two cell membranes an outer membrane and a plasma

membrane. Bar graph representing the inhibition of *E. coli* with respect to the concentration vs zone of inhibition was depicted in Fig. 10. Herewith, our research showed a much more efficient bactericidal function for the sterilization of *E. coli* in a usual existing region (Jing *et al.*, 2018; Janczarek *et al.*, 2018).

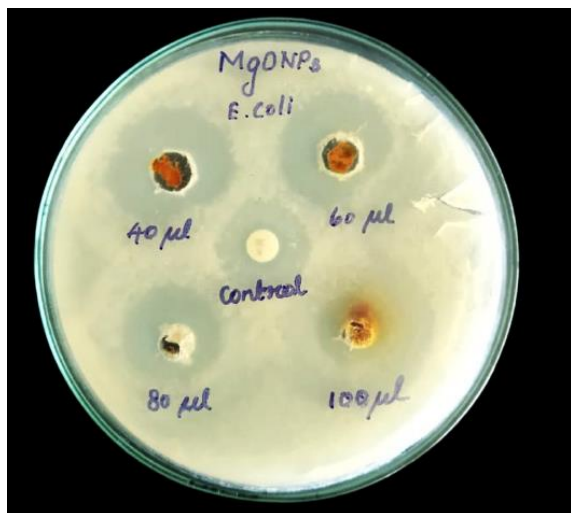


Fig. 9. Antibacterial activity of the synthesized MgONPs.

Table 1. Antibacterial inhibition of the synthesized MgONPs.

Concentration	Zone of Inhibition (mm)	
	Control	<i>E. coli</i>
40	1.8	2.2
60	1.8	2.4
80	1.8	2.5
100	1.8	2.6

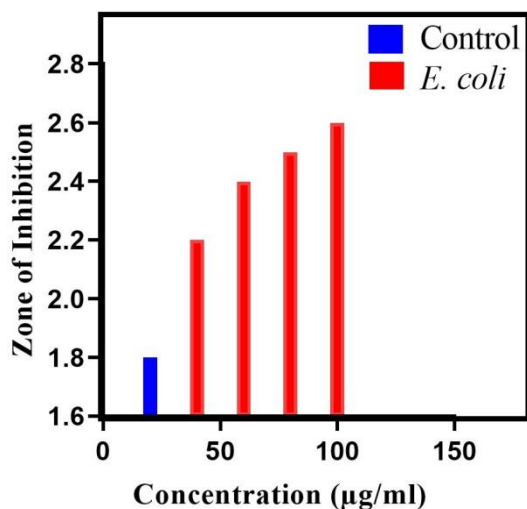


Fig. 10. Inhibition of *E. coli* at increasing concentration of MgONPs.

### Conclusion

The present investigation dealt with the synthesis of MgONPs by the co-precipitation method. Effective destruction of RhB belonging to different chemical groups was achieved by photocatalysis in the presence of MgO suspensions and UV visible light. Our results confirmed that the MgONPs displayed about 90% of degradation within 80 min irradiation time and the antibacterial activity against *E. coli* showed maximum zone formation while increasing the concentration of MgONPs. In the future, the synthesized MgONPs could be used for photocatalytic degradation of toxic dye (RhB) and antibacterial inhibition against *E. coli*.

### Acknowledgment

The authors acknowledge the research center Sri Paramakalyani Centre for Excellence in Environmental Sciences, Manonmaniam Sundaranar University, Alwarkurichi for providing the support for this research work.

### References

- Alavi MA, Morsali A. 2010. Syntheses and characterization of Mg(OH)<sub>2</sub> and MgO nanostructures by ultrasonic method. Ultrasonics Sonochemistry **17(2)**, 441-446.
- AlGaashani R, Radiman S, AlDouri Y, Tabet N, Daud AR. 2012. Investigation of the optical properties of Mg(OH)<sub>2</sub> and MgO nanostructures obtained by microwave-assisted methods. Journal of Alloys and Compounds **521**, 71-76.
- Balamurugan S, Ashna L, Parthiban P. 2014. Synthesis of Nanocrystalline MgO Particles by Combustion Followed by Annealing Method Using Hexamine as a Fuel. Journal of Nanotechnology **2014**, 1-6.
- Bian SW, Baltrusaitis J, Galhotra P, Grassian VH. 2010. A template-free, thermal decomposition method to synthesize mesoporous MgO with a nanocrystalline framework and its application in carbon dioxide adsorption. Journal of Materials Chemistry **20(39)**, 8705.

- Das PS, Dey A, Mandal AK, Dey N, Mukhopadhyay AK.** 2013. Synthesis of Mg(OH)<sub>2</sub> micro/nano flowers at room temperature. *Journal of Advanced Ceramics* **2(2)**, 173-179.
- Devaraja PB, Avadhani DN, Prashantha SC, Nagabhushana H, Sharma SC, Nagabhushana BM, Nagaswarupa HP, Premkumar HB.** 2014. MgO: Eu<sup>3+</sup> red nanophosphor: Low temperature synthesis and photoluminescence properties. *Spectrochimica Acta Part A: Molecular and Biomolecular Spectroscopy* **121**, 46-52.
- Elimelech M, Phillip WA.** 2011. The Future of Seawater Desalination: Energy, Technology, and the Environment. *Science* **333(6043)**, 712-717.
- Ge M, Cao C, Huang J, Li S, Chen Z, Zhang KQ, AlDeyab SS, Lai Y.** 2016. A review of one-dimensional TiO<sub>2</sub> nanostructured materials for environmental and energy applications. *Journal of Materials Chemistry A* **4(18)**, 6772-6801.
- Hvam JM.** 1978. Optical gain and induced absorption from excitonic molecules in ZnO. *Solid State Communications* **26(12)**, 987-990.
- Ibrahim E, Thalij K, Badawy A.** 2017. Antibacterial Potential of Magnesium Oxide Nanoparticles Synthesized by *Aspergillus niger*. *Biotechnology Journal International* **18(1)**, 1-7.
- Janczarek M, Endo M, Zhang D, Wang K, Kowalska E.** 2018. Enhanced Photocatalytic and Antimicrobial Performance of Cuprous Oxide/Titania: The Effect of Titania Matrix. *Materials* **11(11)**, 2069.
- Jiang W, Luo W, Wang J, Zhang M, Zhu Y.** 2016. Enhancement of catalytic activity and oxidative ability for graphitic carbon nitride. *Journal of Photochemistry and Photobiology C: Photochemistry Reviews* **28**, 87-115.
- Jing F, Suo H, Cui S, Tang X, Zhang M, Shen X, Lin B, Jiang G, Wu X.** 2018. Facile synthesis of TiO<sub>2</sub>/Ag composite aerogel with excellent antibacterial properties. *Journal of Sol-Gel Science and Technology* **86(3)**, 590-598.
- Karthik K, Dhanuskodi S, Gobinath C, Prabukumar S, Sivaramkrishnan S.** 2019. Fabrication of MgO nanostructures and its efficient photocatalytic, antibacterial and anticancer performance. *Journal of Photochemistry and Photobiology B: Biology* **190**, 8-20.
- Khan MI, Akhtar MN, Ashraf N, Najeeb J, Munir H, Awan TI, Tahir MB, Kabli MR.** 2020. Green synthesis of magnesium oxide nanoparticles using *Dalbergia sissoo* extract for photocatalytic activity and antibacterial efficacy. *Applied Nanoscience* **10(7)**, 2351-2364.
- Kumar D, Yadav LSR, Lingaraju K, Manjunath K, Suresh D, Prasad D, Nagabhushana H, Sharma SC, Naika HR, Chikkahanumantharayappa, Nagaraju G.** 2015. Combustion synthesis of MgO nanoparticles using plant extract: Structural characterization and photoluminescence studies.
- Lin J, Zeng X, Xiao Y, Tang L, Nong J, Liu Y, Zhou H, Ding B, Xu F, Tong H, Deng Z, Hong X.** 2019. Novel near-infrared II aggregation-induced emission dots for in vivo bioimaging. *Chemical Science* **10(4)**, 1219-1226.
- López R, Gómez R, Llanos, ME.** 2009. Photophysical and photocatalytic properties of nanosized copper-doped titania sol-gel catalysts. *Catalysis Today* **148(1-2)**, 103-108.
- Mahato TH, Prasad GK, Singh B, Acharya J, Srivastava AR, Vijayaraghavan R.** 2009. Nanocrystalline zinc oxide for the decontamination of sarin. *Journal of Hazardous Materials* **165(1-3)**, 928-932.

- Maiti D, Mukhopadhyay S, Devi PS.** 2017. Evaluation of Mechanism on Selective, Rapid, and Superior Adsorption of Congo Red by Reusable Mesoporous  $\alpha$ -Fe<sub>2</sub>O<sub>3</sub> Nanorods. *ACS Sustainable Chemistry & Engineering* **5(12)**, 11255-11267.
- Meshko V, Markovska L, Mincheva M, Rodrigues AE.** 2001. Adsorption of basic dyes on granular activated carbon and natural zeolite. *Water Research* **35(14)**, 3357-3366.
- Min Y, Zhang K, Zhao W, Zheng F, Chen Y, Zhang Y.** 2012. Enhanced chemical interaction between TiO<sub>2</sub> and graphene oxide for photocatalytic decolorization of methylene blue. *Chemical Engineering Journal* **193-194**, 203-210.
- Munawar T, Mukhtar F, Yasmeen S, Naveed-ur-Rehman M, Nadeem MS, Riaz M, Mansoor M, Iqbal F.** 2021. Sunlight-induced photocatalytic degradation of various dyes and bacterial inactivation using CuO-MgO-ZnO nanocomposite. *Environmental Science and Pollution Research* **28(31)**, 42243-42260.
- Pérez Larios A, Lopez R, Hernández Gordillo A, Tzompantzi F, Gómez R, Torres Guerra LM.** 2012. Improved hydrogen production from water splitting using TiO<sub>2</sub>-ZnO mixed oxides photocatalysts. *ISAHOF 2011 Feed and Processes for the Production of Clean Fuels* **100**, 139-143.
- Priyadarshini B, Patra T, Sahoo TR.** 2021. An efficient and comparative adsorption of Congo red and Trypan blue dyes on MgO nanoparticles: Kinetics, thermodynamics and isotherm studies. *Journal of Magnesium and Alloys* **9(2)**, 478-488.
- Pugazhendhi A, Prabhu R, Muruganatham K, Shanmuganathan R, Natarajan S.** 2019. Anticancer, antimicrobial and photocatalytic activities of green synthesized magnesium oxide nanoparticles (MgONPs) using aqueous extract of *Sargassum wightii*. *Journal of Photochemistry and Photobiology B: Biology* **190**, 86-97.
- Pugazhendhi A, Prabhu R, Muruganatham K, Shanmuganathan R, Natarajan S.** 2019. Corrigendum to "Anticancer, antimicrobial and photocatalytic activities of green synthesized magnesium oxide nanoparticles (MgONPs) using aqueous extract of *Sargassum wightii*". *Journal of Photochemistry and Photobiology B: Biology* **195**, 86-97.
- Raliya R, Tarafdar JC, Singh SK, Gautam R, Choudhary K, Maurino VG, Saharan V.** 2014. MgO Nanoparticles Biosynthesis and Its Effect on Chlorophyll Contents in the Leaves of Clusterbean (*Cyamopsis tetragonoloba* L.). *Advanced Science, Engineering and Medicine* **6(5)**, 538-545.
- Saket M, Amini R, Kardar P, Ganjaee M.** 2021. The chemical treatment of the AZ31-Magnesium alloy surface by a high-performance corrosion protective praseodymium (III)-based film. *Materials Chemistry and Physics* **260**, 124113.
- Santhosh C, Velmurugan V, Jacob G, Jeong SK, Grace AN, Bhatnagar A.** 2016. Role of nanomaterials in water treatment applications: A review. *Chemical Engineering Journal* **306**, 1116-1137.
- Sathyamoorthy R, Mageshwari K, Mali SS, Priyadarshini S, Patil PS.** 2013. Effect of organic capping agent on the photocatalytic activity of MgO nanoflakes obtained by thermal decomposition route. *Ceramics International* **39(1)**, 323-330.
- Sharma G, Soni R, Jasuja ND.** 2017. Phytoassisted synthesis of magnesium oxide nanoparticles with *Swertia chirayaita*. *Journal of Taibah University for Science* **11(3)**, 471-477.
- Shi LE, Li ZH, Zheng W, Zhao YF, Jin YF, Tang, ZX.** 2014. Synthesis, antibacterial activity, antibacterial mechanism and food applications of ZnO nanoparticles: a review. *Food Additives & Contaminants: Part A* **31(2)**, 173-186.
- Siedl N, Koller D, Sternig AK, Thomele D, Diwald O.** 2014. Photoluminescence quenching in compressed MgO nanoparticle systems. *Physical Chemistry Chemical Physics* **16(18)**, 8339.

- Song Y, Liu J, Sun K, Xu W.** 2017. Synthesis of sustainable lignin-derived mesoporous carbon for supercapacitors using a nano-sized MgO template coupled with Pluronic F127. *RSC Adv* **7(76)**, 48324-48332.
- Sridewi N, Lee YF, Sudesh K.** 2011. Simultaneous Adsorption and Photocatalytic Degradation of Malachite Green Using Electrospun P(3HB)-TiO<sub>2</sub> Nanocomposite Fibers and Films. *International Journal of Photoenergy* **2011**, 597-854.
- Suresh C, Ningappa C, Nagaveene VM, Umeshreddy K, Girisha KM, Nagabhushana H.** 2017. Photoluminescence properties of Dy 3+-doped LaOF nanophosphor for white LED applications. *Current Science* **113(06)**, 1139.
- Talarposhti A, Mahdavi, Donnelly T, Anderson GK.** 2001. Colour removal from a simulated dye wastewater using a two-phase Anaerobic packed bed reactor. *Water Research* **35(2)**, 425-432.
- Van Dijken A, Meulenkamp EA, Vanmaekelbergh D, Meijerink A.** 2000. The Kinetics of the Radiative and Nonradiative Processes in Nanocrystalline ZnO Particles upon Photoexcitation. *The Journal of Physical Chemistry B* **104(8)**, 1715-1723.
- Van Dijken A, Meulenkamp EA, Vanmaekelbergh D, Meijerink A.** 2000. Influence of Adsorbed Oxygen on the Emission Properties of Nanocrystalline ZnO Particles. *The Journal of Physical Chemistry B* **104(18)**, 4355-4360.
- Veldurthi S, Shin CH, Joo OS, Jung KD.** 2012. Synthesis of mesoporous MgO single crystals without templates. *Microporous and Mesoporous Materials* **152**, 31-36.
- Venkatasubramanian R, Srivastava RS, Misra RDK.** 2008. Comparative study of antimicrobial and photocatalytic activity in titania encapsulated composite nanoparticles with different dopants. *Materials Science and Technology* **24(5)**, 589-595.
- Wang YG, Lau SP, Lee HW, Yu SF, Tay BK, Zhang XH, Hng HH.** 2003. Photoluminescence study of ZnO films prepared by thermal oxidation of Zn metallic films in air. *Journal of Applied Physics* **94(1)**, 354-358.
- Zhou X, Wang X.** 2015. Synthesis, characterization, and luminescence properties of (Li, La)VO<sub>4</sub>/(Li, La)PO<sub>4</sub>: Eu<sup>3+</sup> phosphors. *Optics and Spectroscopy* **118(1)**, 125-130.